

Initial Growth Processes of Ultra-thin Ni-Layers on Si(111) and Electronic Structure of Epitaxially Grown NiSi₂

T. Nishimura, T. Nishimura, J. Takeda, A. Asami, Y. Hoshino and Y. Kido

Abstract

In situ analyses of high-resolution medium energy ion scattering (MEIS) combined with photoelectron spectroscopy clarify the initial growth processes of Ni on Si(111) as-grown and post-annealed. For as-deposition at room temperature, a thin NiSi₂-like layer is initially formed at the interface. With increasing Ni-coverage the surface becomes Ni-rich silicides and finally a Ni layer stacks on the silicide layer for Ni-coverage more than 10 ML. Present MEIS and Si 2p core level analyses reveal the fact that a small amount of Si (~0.7 ML) is incorporated in the Ni-layer and partly segregated to the surface. For the samples with Ni-coverage more than 3 ML, annealing at 500°C leads to formation of a NiSi₂ epitaxial layer, onto which a small amount (~0.2 ML) of Si adatoms are located. Three components observed in the Si 2p spectra with binding energies of 98.8, 99.3 and 99.9 eV scaled from the Fermi level are assigned, respectively to (1)the 1st-layer Si atoms bonded to the Si adatoms, (2)the Si adatoms together with the 1st- (non-bonded to the Si adatoms) and 3rd-layer Si atoms and (3)the bulk NiSi₂ (4th and deeper layers Si atoms). Furthermore, angle-resolved photoemission analysis has derived the bulk band structure along the Γ -L direction and also found a surface state with a strong p_z character, corresponding to the p orbitals of a Si dangling bond.

Department of Physical Sciences, Faculty of Science and Engineering, Ritsumeikan University, Kusatsu, Shiga-ken 525-8577, Japan

1. Introduction

There are numerous reports on the initial growth process for Ni-deposited Si substrates before and after annealing from view points of application to device fabrications and also of fundamental interest[1-5]. In spite of many efforts, the structure and reaction kinetics for the Ni-Si system are not yet understood well. In fact, for deposition at room temperature (RT), surface extended X-ray absorption fine structure (SEXAFS) analysis[6] showed formation of type B NiSi₂ layers for Ni-coverage up to 3 ML(1 ML: 7.83×10^{14} atoms/cm² for Si(111)) and increase in substitutional Ni defects for Ni coverage above 3 ML. Tung and Schrey[7] reported that deposition of a few ML of Ni followed by codeposition of Ni and Si (Ni : Si = 1 : 2) at RT led to formation of epitaxial type B NiSi₂. On the other hand, low and medium energy ion scattering spectroscopy[8,9] indicated formation of islands with average composition of Ni₂Si which are covered with sub-monolayers of amorphous Si for Ni coverage up to about 10 ML. It was also reported that valence band spectra for Ni coverage of 10 ML showed formation of mainly NiSi[10].

In the case of annealing at temperatures from 400 to 600°C, NiSi₂ layers grow epitaxially. Several reports [10-13] suggested that ordered Si cap layers were located on top of the NiSi₂ epitaxial layers just like CoSi₂/Si(111)[14-15]. On the other hand, Vrijmoeth et al.[16,17] concluded a bulk-like termination with a Si-Ni-Si triple layer (TL) and ruled out the existence of the Si overlayers. However, scanning tunneling microscope (STM) observation showed an unreconstructed 1×1 surface with Si adatoms making mainly trimers[18,19]. Although much attention has been paid on metal/Si systems, it is surprising that the valence and core level spectra have been scarcely observed.

Previously, we reported the initial growth process for Ni(1 ML)/Si(111)[20]. In this study, we clarify the structure and reaction kinetics of ultra-thin Ni layers on Si(111) substrate by high resolution medium energy ion scattering (MEIS) combined with photoelectron spectroscopy (PES) using synchrotron (SR) radiation light[21,22]. The former determines elemental depth profiles together with atomic ordering and the latter gives the information about electronic states including chemical shifts. The clean surfaces were prepared by heating at 1200°C in ultra-high vacuum (UHV) after conventional chemical treatments and confirmed by reflection high energy electron diffraction (RHEED). Ni and Si were deposited by molecular beam epitaxy (MBE) with the coverage from 1 up to 50 ML at a deposition rate of 0.5 - 2 ML/min. All the analyses were performed basically *in situ* under UHV conditions.

2. Experiment

Sample pieces with a typical size of 10×10 mm² were cut from on-axis B-doped Si(111)

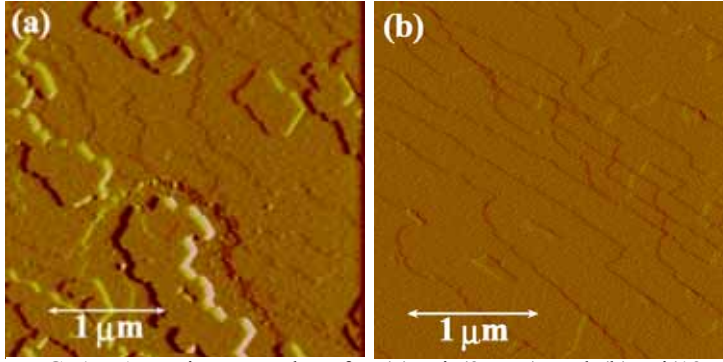


FIG. 1 AFM images taken for (a) Ni (3 ML) and (b) Ni(12 ML) on Si(111) post-annealed at 500°C for 2 min.

wafers. Heating at 1200°C for a few min by infrared radiation after conventional chemical treatment led to clean surfaces showing the 7×7 RHEED pattern. Ni-deposition and co-deposition of Ni and Si were carried out by MBE with Knudsen cells at deposition rates of 0.5 – 2 ML/min. The samples prepared

were (i) Ni deposition at room temperature (RT) followed by annealing at 300, 500 and 700°C and (ii) Ni deposition of 3 Å ($1\text{Å} = 9.14 \times 10^{14} \text{atoms/cm}^2$) followed by co-deposition of Ni and Si (Ni : Si = 1.1 : 2.0) and then annealed at 500°C. The deposition rates for Ni and Si were 0.65 ML/min and 1.2 ML/min, respectively. The surface morphology was observed *ex situ* by an atomic force microscope (AFM) in a contact-mode. Figures 1(a) and (b) show the AFM images observed for Ni(3 & 12 ML)/Si(111) post-annealed at 500°C for 5 min in UHV. The NiSi₂ surface (b) has large terraces and single steps (height: 3.12 Å) of the Si-Ni-Si TL for Ni coverage of 12 ML ($\cong 10 \text{Å}$) and in contrast NiSi₂ islands (a) are seen for Ni coverage of 3 ML.

MEIS and SR-PES analyses were performed *in situ* at beamline 8 named SORIS at Ritsumeikan SR Center[21]. Well collimated 120 keV He⁺ beams impinged on a sample surface and a toroidal electrostatic analyzer (ESA) detected backscattered He⁺ ions with an excellent energy resolution ($\Delta E / E$) of 9×10^{-4} [22]. The depth resolution was estimated to be a few Å. A sample was mounted on a six-axes goniometer and the toroidal ESA was fixed on a turn table. Thus we could easily set any channeling and blocking geometries. In order to suppress secondary electrons emission, +90 V was applied to the sample and the beam current was conducted to ground via an ammeter. Thus the accuracy in the measure of integrated beam current was estimated within several %. The absolute amounts of Ni and Si deposited were calibrated by Rutherford backscattering (RBS) with 1.5 MeV He⁺ beams. Irradiation with monochromated SR photons (10 – 500 eV) excited photoelectrons, which were analyzed by a hemispherical ESA with total energy resolution (ΔE) of about ± 0.1 eV. The exact photon energy was calibrated using the 2nd harmonic wave. All the systems worked under UHV condition better than 2×10^{-10} Torr.

3. Results and Discussion

A. As-grown on Si(111) at RT

The Ni coverage on Si(111) substrates was varied from 1 up to 50 ML. For Ni coverage of 1 ML, the RHEED pattern showed a weak 7×7 structure, which disappeared completely for Ni coverage above 3 ML. Figure 2(a) shows the MEIS spectra observed for 120 keV He^+ ions incident along the [001]-axis and backscattered to the [110] direction of the Si(111) substrate for Ni coverage from 5 up to 40 Å (1 Å

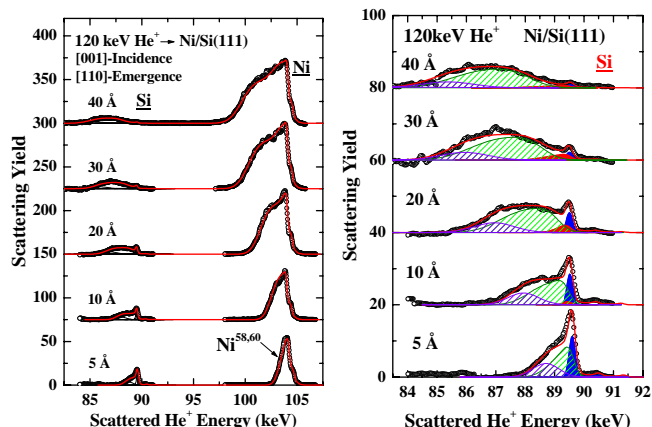


FIG. 2. (a) MEIS spectra observed for 120 keV He^+ ions incident along the [001] axis and backscattered to the [110] direction for Ni coverage of 5, 10, 20, 30 and 40 Å on Si(111). (b) Magnified MEIS spectra from Si. Red curves are the best-fitted spectra assuming appropriate elemental depth profiles. Filled blue and red areas are the components from Si on top and incorporated in Ni layer, respectively. Slashed green and purple areas deconvoluted come from Ni-silicide and Si substrate, respectively.

= 1.17 ML). The open circles denote the observed spectra and the solid curves are the best-fitted ones assuming appropriate layered structures with thickness fluctuations. The stopping powers of Si and Ni were determined in advance using amorphous Si and Ni films stacked on Si(111) substrates whose thicknesses were calibrated by RBS using 1.5 MeV He^+ beams. In order to judge whether a layered or islands structure is formed, reliable energy straggling values are indispensable. Unfortunately, however, it is difficult to measure energy straggling precisely due to film-thickness fluctuation and existence of fine crystallites[23,24]. Stopping powers and the fluctuations were also calculated mainly based on the dielectric response theory[25-27]. However, the theoretical predictions are significantly discrepant each other. In the present MEIS analysis, we multiplied the Ziegler's semi-empirical stopping powers[28] by correction coefficients which were estimated from those determined experimentally. Concerning the energy straggling, the Bohr straggling values were multiplied by appropriate damping coefficients, which were estimated from the data base accumulated so far for various kinds of samples. In the MEIS spectrum simulation, it is convenient to have analytical expressions of the stopping power and energy straggling as a function of He ion velocity.

Figure 2(b) indicates the magnified MEIS spectra from Si observed and best-fitted. For Ni coverage 5 and 10 Å, the surface consists of Ni-silicide layer, on which a small amount of Si atoms are segregated. With increasing Ni coverage, the silicide becomes Ni-rich. The average elemental composition of the silicide layer is Ni_2Si at Ni coverage of 10 Å. For Ni coverage more than 10 Å, a Ni-layer grows on the silicide layer and contains a small amount

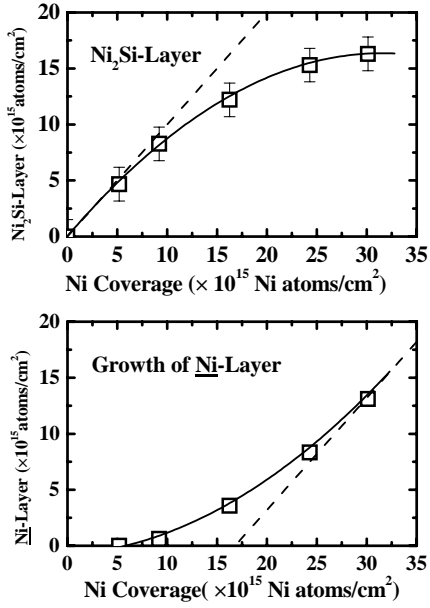


FIG. 3. Thickness of Ni-silicide layer (top) (Ni_2Si is assumed) and of Ni layer (bottom) stacking on the silicide layer as a function of Ni-coverage. Curves are drawn for guide the eyes. Linear lines (dotted) indicate uniform stacking of Ni_2Si (upper) and Ni (bottom) layers only.

The Ni-layer starts to stack on the silicide layer at Ni coverage of 10 Å and the Ni-silicide layer continues to grow up to Ni coverage of 30 Å. In fact, Ni lattices were seen weakly in the RHEED patterns for Ni coverage more than 20 Å.

We observed Si $2p_{1/2,3/2}$ core level spectra at photon energy of 110, 140, and 280 eV. Figure 4 shows the Si $2p$ spectra observed at photon energy of 140 eV under normal emission

condition for Ni coverage 0.86, 2.6, 5, 10 and 20 Å. Here, the binding energy (E_B) is scaled from the Fermi level (E_F). For Ni coverage of 0.86 and 2.6 Å, the spectra consist of three peaks. The Si bulk component is assigned to that with E_B of 99.45 eV, which is dominant at photon energy of 280 eV due to a considerably larger escape depth. The component with a higher E_B of 99.9 ± 0.1 eV would come from the NiSi_2 phase. In fact, as will be shown later, the Si $2p$ spectra from the type B $\text{NiSi}_2(111)$ grown by post-annealing have a binding energy of 99.9 ± 0.1 eV. The Ni K -edge SEXAFS analysis[6] asserted that

of Si (red). The amount of Si segregated on top of the surface (blue) gradually decreases with increasing Ni coverage but still exists for Ni-coverage of 40 Å. Total amount of Si atoms segregated on top of the surface and incorporated in the Ni-layer is almost constant about 0.65 ± 0.15 ML. They probably originate from the Si adatoms (0.37 ML) together with Si atoms around corner holes of the 7×7 surface and partly from the Si atoms in the silicide layer substituted by Ni. As will be shown later, the above two Si components were clearly observed separately in the Si $2p$ spectra. Figure 3 indicates the thickness of the Ni-silicide layer (Ni_2Si was assumed as average composition) (top) and of the Ni-layer (bottom) on the silicide layer as a function of Ni coverage.

The Ni-layer starts to stack on the silicide layer at

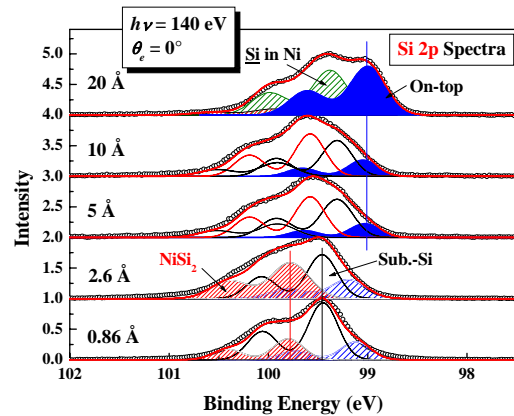


FIG. 4. Si $2p_{1/2,3/2}$ core level spectra observed at photon energy of 140 eV under normal emission condition for Ni coverage of 0.86, 2.6, 5, 10 and 20 Å. Observed spectrum was deconvoluted into components from Si on top (filled blue area), incorporated in Ni (slashed green area) and NiSi_2 (slashed red area). The binding energy for Si substrate was determined at photon energy of 280 eV (2nd harmonic wave). The blue, black and red bars indicate the energy positions (Si $2p_{3/2}$) for the surface-segregated Si, bulk Si and NiSi_2 , respectively.

type B NiSi₂-like structure is initially formed and the intensity of the NiSi₂ phase decreases with increasing the Ni coverage up to 5 ML due to progressive Ni substitution with the Si atoms within the NiSi₂ overlayer. The component with the lowest binding energy of 99.1±0.05 eV (Ni coverage 0.86 Å) and of 99.2±0.05 eV (Ni coverage 2.6 Å) may originate from surface-segregated Si on the NiSi₂ overlayer and/or top Si atoms of the Si-Ni-Si TL. This is also expected from the Si 2p spectra observed for the post-annealed samples, discussed later. The present result is consistent with the structure model based on the above SEXAFS analysis. We observed epitaxial growth of type B NiSi₂ layers on Si(111) even at RT by pre-deposition of 3 ML of Ni followed by co-deposition of NiSi₂, as reported by Tung and Schrey[7]. This indicates the formation of a template of type B NiSi₂ by Ni pre-deposition and supports the formation of the type B NiSi₂ layer at the interface.

The Si 2p spectra observed for Ni coverage of 5 and 10 Å resemble each other and are deconvoluted into four components. The component with the lowest E_B (99.0±0.1 eV) comes from the surface segregated Si atoms. This is predicted by the present MEIS analysis and by comparison with the Si 2p spectrum observed for Ni coverage of 20 Å. The other three components probably correspond to Ni-silicides, although the deconvolution has some ambiguities. For Ni coverage of 20 Å, the Si 2p spectrum consists of only two components, which are assigned to Si atoms segregated on top of the surface (lower binding energy: 99.0±0.1 eV) and to those incorporated in the Ni layer (99.4±0.1 eV) from the emission angle dependence and the MEIS spectrum analysis. The concentration of Si in the Ni layer was estimated to be 10 at. %. The Si atoms probably take interstitial sites and interact weakly with the Ni lattice, because the RHEED pattern showed stacking of a Ni(111) layer.

Figure 5 shows the valence band (VB) spectra taken at photon energy of 40 eV under normal emission condition. The spectrum for Ni coverage of 2.6 Å (3 ML) resembles that observed previously for bulk NiSi, which has a main broad peak at 1.8 eV (full width at a half maximum: FWHM \cong 2 eV) accompanied by a smaller peak at ~3 eV below E_F corresponding to the NiSi₂ phase[29]. This seems contrary to the Si 2p analysis indicating NiSi₂ formation at the interface. However, as clarified by the SEXAFS analysis[6], progressive Ni substitution with the Si atoms within the NiSi₂ overlayer takes place with increasing the Ni coverage up to 5 ML. Thus the top TL is Ni-rich rather than NiSi₂ (3 ML Ni

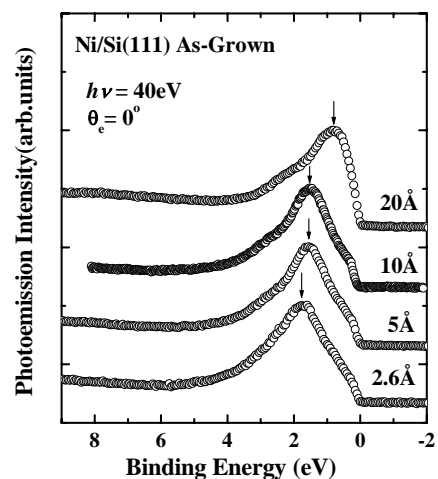


FIG. 5. Valence band spectra observed at photon energy of 40 eV under normal emission condition for Ni coverage of 2.6, 5, 10 and 20 Å. Binding energy is scaled from the Fermi level (E_F).

deposition makes 3 TLs). Unfortunately, the MEIS analysis only gives the average elemental compositions of the ultra-thin silicide layers due to energy straggling and some thickness non-uniformity. However, with increase in Ni coverage, the peak position in the VB spectra shifts toward E_F , indicating more Ni-rich silicide formation, as predicted by Bisi et al.[30]. According to the SR-PES observation by Franciosi et al.[29], a primary peak originating from the Ni d-band is located at 1.3, 1.8 and 3.15 eV below E_F for bulk Ni_2Si , NiSi and NiSi_2 , respectively. For Ni coverage of 20 Å, the VB spectrum has a Ni metal feature. This is consistent with the present MEIS result.

From the above discussion, it is seen that Ni atoms deposited diffuse to the interface to form Ni-silicide layers. In fact, we confirmed that the moving species is Ni atoms by RBS analysis using a marker ($\text{Ni}(500 \text{ Å})/\text{W}(0.5 \text{ Å})/\text{Si}(111)$). On the other hand, the Si adatoms together with Si atoms around the corner holes of the 7×7 surface segregate to the surface and partly incorporated in a stacked Ni layer. A small amount of Si atoms in the silicide layer substituted by Ni may also move toward the surface. Concerning the surface morphology, AFM observation showed thickness fluctuations (standard deviation) of the overlayers about 20 - 30 % for Ni coverage of 10 Å. With increase in Ni coverage, the thickness fluctuations decrease. All the MEIS spectra are best-fitted assuming a layered structure. However, due to uncertainty of the energy straggling, we cannot rule out the silicide-islands formation, as reported by van Loenen et al.[8]. Probably Ni-silicides islands grow for Ni coverage less than 5 Å, because the bulk Si 2p component for Ni coverage of 2.6 Å is much stronger than that estimated for layered stacking.

B. Ni/Si(111) Post-annealed

It is well known that NiSi_2 layers are epitaxially grown by Ni deposition followed by post-annealing at temperatures from 400 up to 600°C. According to the report of Tung[31], Ni-deposition of $10\pm 1 \text{ Å}$ and of $18\pm 1 \text{ Å}$ at deposition rate of $\sim 6 \text{ Å/min}$ followed by annealing at $\sim 500^\circ\text{C}$ led to formation of type B and type A NiSi_2 epitaxial layers, respectively. The best quality of the epitaxial type B NiSi_2 layers is obtained by Ni pre-deposition of 2-3 ML at RT followed by co-deposition of Ni and Si (slightly Ni rich compared with NiSi_2) and then annealed at $\sim 500^\circ\text{C}$ [5]. In general, Ni deposition only on Si(111) followed by annealing tends to form pinholes[5].

In spite of a number of reports on epitaxial NiSi_2 growth on Si(111), the atomic and electronic structures of the surface are still unknown. It is widely believed that the NiSi_2 surface has an additional Si bilayer on top of the last TL just like $\text{CoSi}_2/\text{Si}(111)$ [14,15]. Porter et al.[13] analyzed the epitaxial NiSi_2 surface by low energy impact collision ion scattering spectroscopy (ICISS) and claimed that the surface consisted of a Si bulk

termination with an additional Si bilayer on top. Valence band photoemission study[11] showed Si segregation to the NiSi₂ surface. Hinkel et al.[10] observed the Si 2p spectra using SR-light for the epitaxial NiSi₂/Si(111) and assigned the deconvoluted two components to a Si layer with thickness of 3-5 Å on top (lower binding energy) and to the bulk NiSi₂(111) (higher binding energy). Against the above reports, Vrijmoeth et al.[16,17] analyzed the epitaxial NiSi₂/Si(111) by MEIS using 100 keV H⁺ beams and concluded that the surface was terminated by a Si-Ni-Si TL without additional Si bilayer on top. The epitaxial NiSi₂ surface was also observed by STM. Hasegawa et al.[18] found an unreconstructed 1×1 surface with Si adatoms making mainly trimers. Another STM observation[19] also revealed the surface consisting of monomers, dimmers and trimers.

In this study, our concern is focused on type B NiSi₂ growth on Si(111). The samples prepared are (i) Ni deposition of 10 and 20 Å at RT followed by annealing at 300, 500 and 700°C and (ii) Ni deposition (3 Å) followed by co-deposition of Ni(10Å) and Si(18 Å) and then annealed at 500°C. The formation of the type B NiSi₂ epitaxial layer was confirmed by RHEED. Judging the type A or type B which was dominant was made by asymmetry of the Kikuchi lines at the [110]-azimuth of Si(111) substrate according to the method proposed by Bennett et al.[32]. All the samples annealed at 500°C showed a 1×1 structure. The type B NiSi₂(111) formation was also confirmed by MEIS using the channeling effect for the samples (ii) and Ni(10 Å)/Si(111) annealed at 500°C. On the other hand, as reported by Tung[31], the type A predominates for Ni(20 Å)/Si(111) post-annealed at 500°C.

Figure 6 shows the MEIS spectra observed for 120 keV He⁺ ions incident along the [001] axis and backscattered to the [110] direction of Si(111) substrate on which type B NiSi₂(111) layer is epitaxially grown (sample (ii)). The upper spectrum comes from Ni and the bottom from Si. Under such a double alignment geometry, the normalized scattering yield (hitting probability) from the 5th-layer Ni to that from the 2nd-layer Ni is estimated to be ~0.1. The normalized scattering yields for the 3rd- and 4-th layers Si are also derived to be 0.63 and

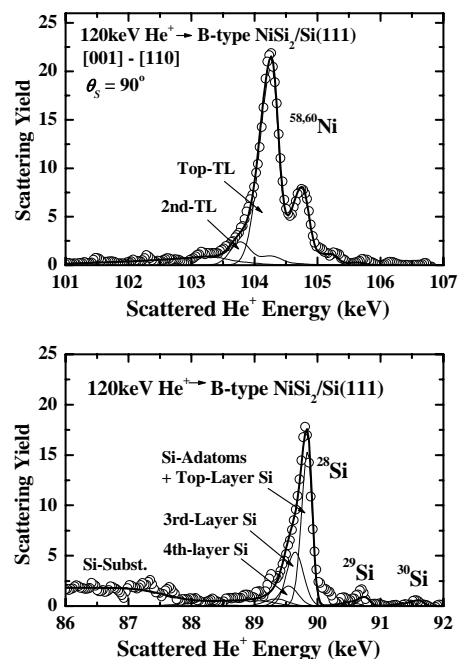


FIG. 6. MEIS spectra observed for 120 keV He⁺ ions incident along the [001] axis and backscattered to [110] direction of Si(111) from type B NiSi₂(111)/Si(111). The top spectrum comes from Ni and the bottom from Si. Thick and thin curves are the best-fitted total and deconvoluted spectra.

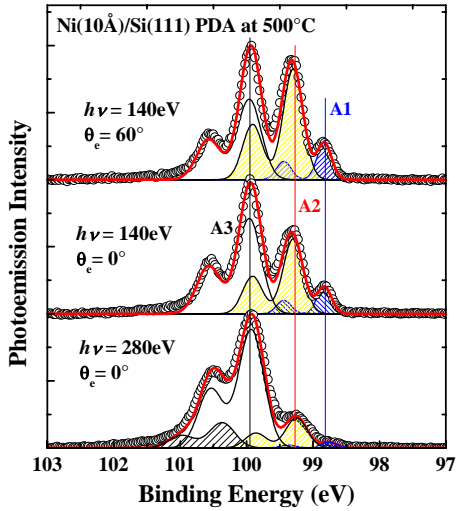


FIG. 7. Si 2p core level spectra observed for Ni(10Å)/Si(111) post-annealed at 500°C for 2 min at photon energy of 140 and 280 eV (at [110]-azimuth). Top, middle and bottom spectra correspond to emission angle (θ_e scaled from surface normal) of 0° and 60° at 140 eV and of 0° at 280 eV, respectively. The red and blue bars indicate the energy positions (Si 2p_{3/2}) of surface-related components and the black bar the energy position of the NiSi₂ bulk. The hatched component is required to reproduce the spectrum observed at photon energy of 280 eV.

amount of the Si-adatoms be $x(\text{ML})$. Then, we have $0.79/(1+x) = 0.63$ and $0.3/(1+x) = 0.26$, if we assume no shadowing effect of the Si-adatoms on the 3rd- and 4th- layers Si. From the above equations, $x \cong 0.2 \text{ ML}$ is deduced. Thus the present MEIS result rules out the existence of the Si bilayer on top and supports the Si-Ni-Si bulk-like termination accompanied by a small amount of Si adatoms, which probably make monomers, dimmers and trimers, as observed by STM[18,19].

Figure 7 shows the Si 2p_{1/2,3/2} core level spectra observed for Ni(10Å)/Si(111) post-annealed at 500°C for 2 min at photon energy of 140 eV (emission angle scaled from surface normal: $\theta_e = 0$ and 60°) and at 280 eV ($\theta_e = 0^\circ$: normal emission). The spectra have three components (A1, A2, A3) with binding energy of 98.8, 99.3 and 99.9 eV with uncertainty of ± 0.1 eV. The energy and emission angle dependence assigns the component with binding energy of 99.9 eV (A3) to the bulk NiSi₂ and the other two components originate from surface-related ones. We evaluated the Mulliken charges[33] of the Si adatoms (monomers and trimers are assumed) and the underlying two TLs by the *ab initio* calculations (CASTEP code[34]). As a result, the Mulliken charges of the Si adatoms, the 1st-layer Si atoms bonded and non-bonded to the Si adatoms are 0.20 ± 0.03 , 0.0 ± 0.1 , and 0.20 ± 0.05 , respectively. The Mulliken charge of the 3rd-layer Si atoms (0.21 ± 0.03) is significantly lower than that of the 4th and deeper layers Si atoms (0.30 ± 0.03). Thus the component with the lowest binding energy (A1: 98.8 eV) corresponds to the 1st-layer Si atoms bonded to the

0.26, respectively. Here, we assumed that each scattering component takes approximately an asymmetric Gaussian shape. If one assumes the bulk-like termination of TL and employs the root mean square thermal vibration amplitudes of 0.095 and 0.110 Å for the Ni and Si atoms in the silicide, respectively[17], the hitting probabilities for the 5th-layer Ni and the 3rd- and 4th-layers Si are calculated to be 0.08, 0.79 and 0.3, respectively. The hitting probability calculated for the 5-th layer Ni is consistent with the MEIS result. As shown below, the Si 2p spectra suggest the presence of small amount of Si adatoms on top. Now, let the

Si adatoms and the another component (A2: 99.3 eV) comes from the Si adatoms, the 1st-layer Si atoms non-bonded to the Si adatoms, and the 3rd layer Si. Of course, the Mulliken charge does not express absolutely the real charge state of lattice site atoms and the core level shift reflects both initial and final states of the excited electron[35]. However, it is effective to assign relative core level shifts. The intensity ratio of A1, A2 and A3 is $A1 : A2 : A3 \cong 1 : 4 : 6$, which was observed at photon energy of 140 eV under normal emission condition. Assumption of the above assignment (Si adatoms: 0.2 ML) and the escape depth of 4-5 Å[10] reproduces well the observed intensity ratio. No significant difference was seen in the Si 2p spectra observed at normal emission for Ni(10 Å)/Si(111) and Ni(20 Å)/Si(111) post-annealed at 500°C and the sample (ii). This indicates no difference in the kinetic processes of the surface segregation of Si during the type A and type B interface-formation. For the Si 2p spectrum observed at photon energy of 280 eV, an additional peak with the highest binding energy is seen (see Fig. 7). This component is required to reproduce the Si 2p spectra observed at higher photon energy. This may be responsible for transfer of a valence electron from Ni to Si, expected based on a molecular orbital description, just like a satellite line[36].

We deposited Si with coverage of 1 ML on the NiSi₂(111) surface at RT. Stacking of one ML Si on top gives an additional component in the Si 2p spectra. After annealing at 500°C for 2 min in UHV again, the Si 2p spectra observed coincided well with those before the Si post-deposition. A quite same event takes place for Ni deposition of 0.6 ML on NiSi₂(111) at RT and then annealing at 500°C. It is seen that annealing at 500°C evaporates completely the post-deposited Si and Ni atoms on top and does not lead to any chemical reactions. This indicates that the Si adatoms probably making monomers, dimmers and trimers were segregated to the surface during the initial silicidation and then stabilized by being bonded to the 1st layer Si atoms of the top Si-Ni-Si TL.

Annealing-temperature dependent Si 2p spectra observed at normal emission for Ni(10 Å)/Si(111) are shown in Fig. 8. All the spectra from the samples post-annealed at 300, 500 and 700°C consist of three components, corresponding to A1, A2 and A3. Three components for the sample

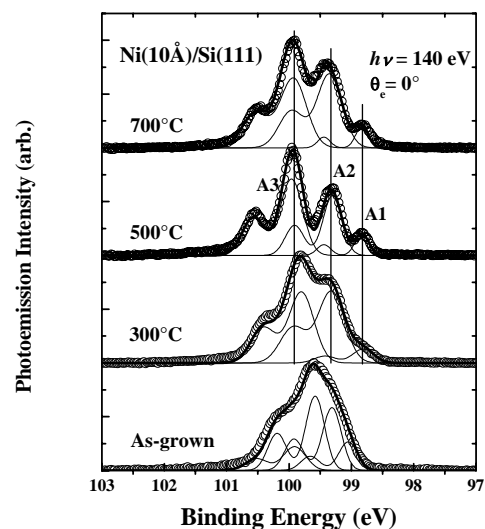


FIG. 8. Si 2p core level spectra observed at photon energy of 140 eV for Ni(10 Å)/ Si(111), as-grown, post-annealed at 300, 500 and 700°C for 2 min. Detection angle was set to $\theta_e = 0^\circ$ (normal emission). The blue, red and black lines indicate the peak positions (Si 2p_{3/2}) for A1, A2 and A3 components, respectively (see Fig. 7).

annealed at 300°C are significantly broadened and the bulk component (A3) shifts toward the lower binding energy side. This indicates multi-silicide phase formation, although primary phase is NiSi₂. Annealing at 700°C results in no peak shifts compared with that observed for the sample annealed at 500°C but the widths of the two components A2 and A3 become broad. This suggests that the epitaxial NiSi₂ layer starts to decompose partly.

C. Electronic Band Structure of NiSi₂(111)

Figure 9 indicates the VB spectra for Ni(10Å)/Si(111) annealed at 500°C taken at photon energy of 40 eV by varying detection angles. The peaks observed are classified into surface and bulk electronic states. The former originates mainly from two-dimensional boundary conditions. Four peaks (S1 - S4) near E_F come from surface state levels, because their intensities are considerably reduced by exposure to O₂ and no dispersion was observed for wave vectors along Γ -L direction. Three components denoted by B1, B2 and B3 correspond

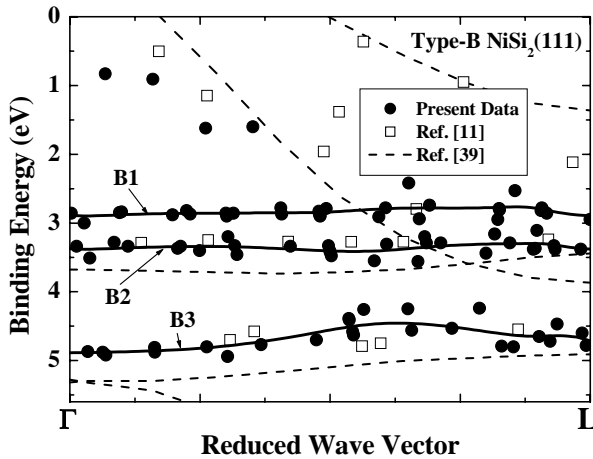


FIG. 10. Bulk (NiSi₂) band structure along Γ -L in the first Brillouin zone. Full circles and open squares, respectively denote the present data and those observed by Chang and Erskine[11]. Solid curves are drawn to guide the eye. Dashed curves denote the theoretical predictions based on the linear-muffin-tin-orbital method[40]. Parabolic curves (dotted) drawn originate from s- and p-orbitals, indicating a free-electron-like nature.

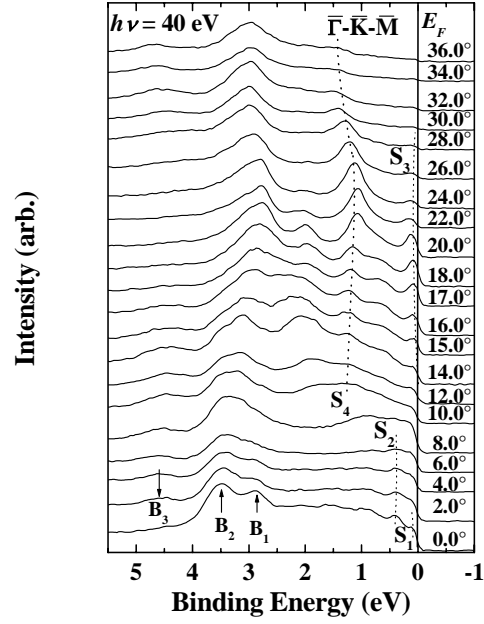


FIG. 9. Valence band spectra observed by varying detection angle at photon energy of 40 eV for Ni(10 Å)/Si(111) annealed at 500°C (at [1 1 0]-azimuth).

to the NiSi₂ bulk band and are energetically localized around 2.7-2.9, 3.3-3.8 and 4.3-4.9 eV, respectively. Thus they would originate mainly from the Ni 3d state. So far, the NiSi₂ bulk band structure was calculated by self-consistent linear augmented-plane wave[37], self-consistent linear combination of Gaussian orbitals[38] and linear-muffin-tin orbitals method[39,40]. The results are almost coincident with each other. The bulk band structure for wave vectors along Γ -L is indicated in Fig. 10 and compared with the theoretical

predictions[39]. Here, we deduced the a crystal potential V_0 to be 14.3 eV by employing the Bragg plane method[41]. All the three dispersion curves are almost parallel each other. The B2 and B3 energy dispersions observed here correspond to the Ni 3d band calculated from the above theoretical models. However, the B1 state is not predicted theoretically but probably originates from the Ni 3d orbitals because of its localized nature. In fact, the B1 peak is independent of polarization of incident photon (not dangling bond state) and insensitive to oxygen-exposure and its dispersion does not coincide with the surface periodicity in the extended surface Brillouin zone. We calculated the electronic states by the CASTEP code[34] for four Si-Ni-Si triple layers. As a result, it is found that the B3 state consists of Si 2p (~50 %) and Ni 3d (~50 %) and the B2 state (Ni 3d: 100 %) is split into two branches B1 and B2.

We also derived the dispersion relations for the surface states (S1 - S4) by angle-resolved photoemission analysis, as shown in Fig. 11. The dashed curve indicates the calculations for the bulk terminated surface reported by Manghi et al.[40]. Such a surface state level does not appear for the surface terminated with the Si bilayer[40]. We observed the peak intensity of S3, S4 and B1-B3 dependent on polarization of the incident photon (*s*- and *p*-polarization).

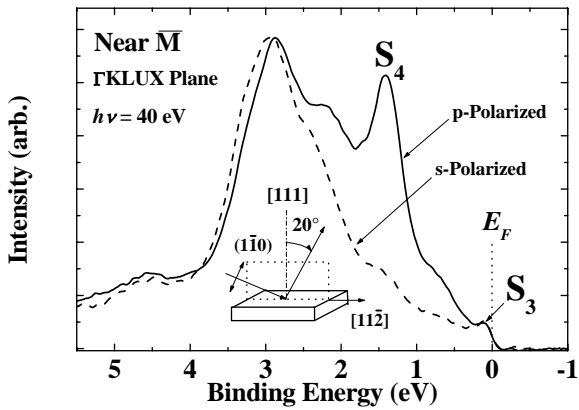


FIG. 12. Valence band spectra taken with *s*- (normal incidence: dashed curve) and *p*-polarized (incidence at 70°: solid curve) lights at photon energy of 40 eV.

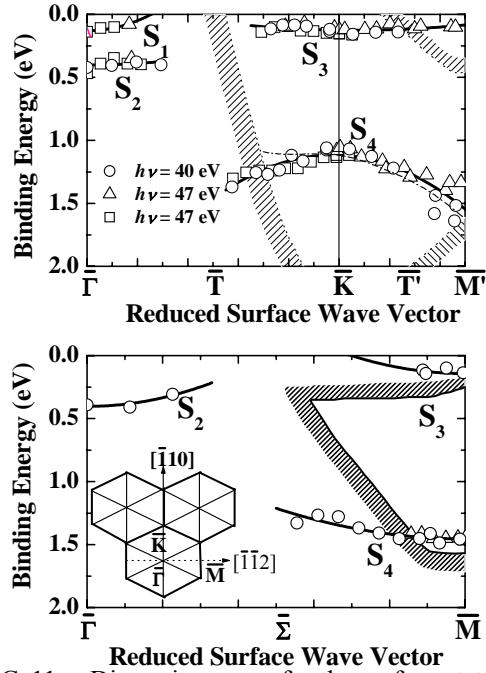


FIG. 11. Dispersion curve for the surface state level (S4) for type B $\text{NiSi}_2(111)$ along $\Gamma - T - M$ (top) and along $\Gamma - \Sigma - M$ (bottom). The dashed curve denotes theoretical prediction by Manghi et al.[40] for the bulk-truncated $\text{NiSi}_2(111)$ surface. The shades areas indicate the projection of the bulk bands. The solid curves are drawn to guide the eyes.

As a result, only the S4 state has a strong p_z character, as shown in Fig. 12. Therefore, this S4 state corresponds to the *p* orbitals localized on top-layer Si atoms, namely a Si dangling bond, as theoretically predicted[40].

Finally, we determined the work function of the type B $\text{NiSi}_2(111)$ surface. Figure 13 shows the VB spectrum as a function of kinetic energy of emitted photoelectrons taken at photon energy of

39.8 eV (at $[11\bar{2}]$ -azimuth) under normal emission condition. Here, a negative bias of -6.27 V was applied to the sample. The work function of the sample (Φ_{NS}) is expressed by

$$h\nu = E_{kin}^F - E_{kin}^0 + \Phi_{NS}, \quad (1)$$

where $h\nu (= 39.8$ eV), E_{kin}^F and E_{kin}^0 , respectively are incident photon energy, kinetic energy of photoelectrons excited from the state with the Fermi energy and the cut-off kinetic energy of secondary electrons (see Fig. 13). We varied the bias voltage

from -2.0 V down to -8.0 V and measured the E_{kin}^F and E_{kin}^0 values at the same incident photon energy. The work function of the type B $\text{NiSi}_2(111)$ is deduced to be 5.07 ± 0.05 eV, which coincides well with the value of 5.05 eV measured by Chang and Erskine[11] but significantly larger than that of 4.64 eV reported by Wissman et al.[42]. The value obtained here is slightly smaller than that of $\text{Ni}(111)$ (5.22 eV).

4. Summary

In situ analyses of high-resolution MEIS and PES have clarified the initial growth processes of Ni on Si(111) substrates. For as-deposition at RT, a thin NiSi_2 -like layer is initially formed at the interface. With increasing Ni-coverage the surface becomes Ni-rich silicides and a Ni layer starts to stack on the silicide layer for Ni-coverage more than 10 ML. Present MEIS analysis reveals the fact that a small amount of Si (~ 0.7 ML) is incorporated in the Ni-layer and partly segregated to the surface. These two components have distinct peaks in the Si 2p spectra and that with a lower binding energy (99.0 ± 0.1 eV) is assigned to the Si atoms segregated to the surface and another (99.4 ± 0.1 eV) to those incorporated in the Ni layer.

For the samples with Ni-coverage more than 3 ML, annealing at 500°C leads to formation of a NiSi_2 epitaxial layer, onto which a small amount (~ 0.2 ML) of Si adatoms are located, namely no Si bilayers on top. We found clearly three components in the Si $2p_{3/2}$ spectra with binding energies of 98.8 , 99.3 and 99.9 eV, which are assigned, respectively to (1) the 1st-layer Si atoms bonded to the Si adatoms, (2) the Si adatoms together with the 1st- (non-bonded to the Si adatoms) and 3rd-layer Si atoms and (3) the bulk NiSi_2 (4th and deeper

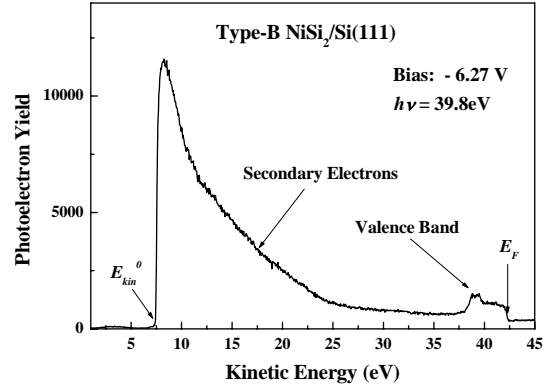


FIG. 13. Valence band spectrum observed at photon energy of 39.8 eV under normal emission condition for type B $\text{NiSi}_2(111)$ surface prepared by Ni-Si co-deposition (sample (ii)). The sample was negatively biased at -6.27 V.

layers Si atoms). Furthermore, angle-resolved photoemission analysis has revealed the surface states together with three bulk states. The bulk band structure along the Γ -L direction is energetically localized and originates mainly from Ni 3d states. A newly found bulk-like state coincides with that derived by the first principles calculations (CASTEP). One of the surface states (S4: 1.0 – 1.5 eV below E_F) observed here has a strong p_z character, corresponding to the p orbitals of a Si dangling bond, which agrees with that theoretically predicted for the bulk-terminated NiSi₂(111) surface.

Acknowledgements

The authors would like to thank Prof. T. Nakada for observing the surface morphology of NiSi₂/Si(111) by AFM. Thanks are also due to Prof. H. Namba and Dr. K. Ogawa for maintaining the PES analysis system.

References

- [1] N.W. Cheung, R.J. Culbertson, L.C. Feldman, P.J. Silverman, K.W. West and J.W. Mayer, Phys. Rev. Lett. **45** (1980) 120.
- [2] R.T. Tung, J.M. Gibson and J.M. Poate, Phys. Rev. Lett. **50** (1983) 429.
- [3] E.J. van Loenen, J.W.M. Frenken, J.F. van der Veen, and S. Valeri, Phys. Rev. Lett. **54** (1985) 827.
- [4] J.M. Gibson and J.L. Batstone, Surf. Sci. **208** (1989) 317.
- [5] R.T. Tung, *Handbook of Semiconductors*, (North-Holland, Amsterdam, 1994) Chapt. 25.
- [6] F. Comin, J.E. Rowe and P.H. Citrin, Phys. Rev. Lett. **51** (1983) 2402.
- [7] R.T. Tung and F. Schrey, Appl. Phys. Lett. **55** (1989) 256.
- [8] E.J. van Loenen, J.F. van der Veen and F.K. LeGoues, Surf. Sci. **157** (1985) 1.
- [9] T.L. Porter, C.S. Chang, U. Knipping and I.S.T. Tsong, Phys. Rev. **B 36** (1987) 9150.
- [10] V. Hinkel, L.Sorba, H. Haak, K. Horn and W. Braun, Appl. Phys. Lett. **50** (1987) 1257.
- [11] Y.-J. Chang and J.L. Erskine, Phys. Rev. **B 26** (1982) 7031.
- [12] S.C. Wu, Z.Q. Wang, Y.S. Li, F. Jona and P.M. Marcus, Solid State Commun. **57** (1986) 687.
- [13] T.L. Porter, D.M. Cornelison, C.S. Chang and I.S.T. Tsong, J. Vac. Sci. Technol. **A 8** (1990) 2497.
- [14] S.A. Chambers, S.B. Anderson, H.W. Chen and J.H. Weaver, Phys. Rev. **B 34** (1986) 913.
- [15] J.E. Rowe, G.K. Wertheim and R.T. Tung, J. Vac. Sci. Technol. **A 7** (1989) 2454.
- [16] J. Vrijmoeth, P.M. Zagwijn, J.W.M. Frenken and J.F. van der Veen, Phys. Rev. Lett. **67** (1991) 1134.

- [17] J. Vrijmoeth, P.M. Zagwijn, E. Vlieg, J.W.M. Frenken and P.F.A. Alkemade, *Surf. Sci.* **290** (1993) 255.
- [18] Y. Hasegawa, Y. Kuk, R.T. Tung, P.J. Silverman and T. Sakurai, *J. Vac. Sci. Technol.* **B 9** (1991) 578.
- [19] J.A. Kubby and W.J. Greene, *J. Vac. Sci. Technol.* **A 12** (1994) 2009.
- [20] Y. Hoshino, T. Nishimura, Y. Taki, Y. Asami, K. Sumitomo and Y. Kido, *Surf. Sci.* **511** (2002) 112.
- [21] Y. Kido, H. Namba, T. Nishimura, A. Ikeda, Y. Yan and A. Yagishita, *Nucl. Instrum. Methods* **B 136-138** (1998) 798.
- [22] T. Nishimura, A. Ikeda and Y. Kido, *Rev. Sci. Instrum.* **69** (1998) 1671.
- [23] Y. Kido and T. Koshikawa, *Phys. Rev.* **A 44** (1991) 1759.
- [24] K. Sumitomo, T. Nishioka, A. Ikeda and Y. Kido, *Phys. Rev.* **B 56** (1997) 7011.
- [25] J. Lindhard and A. Winther, *K. Dan. Vidensk. Selsk. Mat.-Fys. Medd.* **34** No.4 (1964) 1.
- [26] I. Gertner, M. Meron and B. Rosner, *Phys. Rev.* **A 18** (1978) 2022.
- [27] T. Kaneko, *Phys. Rev.* **A 33** (1986) 1602.
- [28] J.F. Ziegler, *He Stopping Powers and Ranges in All Elements* (Pergamon, New York, 1977).
- [29] A. Franciosi, J.H. Weaver and F.A. Schmidt, *Phys. Rev.* **B 26** (1982) 546.
- [30] O. Bisi, L.W. Chiao and K.N. Tu, *Phys. Rev.* **B 30** (1984) 4664.
- [31] R.T. Tung, *J. Vac. Sci. Technol.* **A 5** (1987) 1840.
- [32] P.A. Bennett, A.P. Johnson and B.N. Halawith, *Phys. Rev.* **B 37** (1988) 4268.
- [33] R.S. Mulliken, *J. Chem. Phys.*, **23** (1955) 1833.
- [34] M.C. Payne, M.P. Teter, D.A. Allan, T.A. Arias and J.D. Joannopoulos, *Rev. Mod. Phys.* **64** (1992) 1045.
- [35] E. Pehlke and M. Scheffler, *Phys. Rev. Lett.* **71** (1993) 2338.
- [36] S. Asada and S. Sugano, *J. Phys. Soc. Jpn.* **41** (1976) 1291.
- [37] Y.J. Chabal, D.R. Hamann, J.E. Rowe and M. Schlüter, *Phys. Rev.* **B 25** (1982) 7598.
- [38] D. M. Bylander, L. Kleinman, K. Mednick and W.R. Grise, *Phys. Rev.* **B 26** (1982) 6379.
- [39] W.R.L. Lambrecht, N.E. Christensen and P. Blöchl, *Phys. Rev.* **B 36** (1987) 2493.
- [40] F. Manghi, G. Guidetti and O. Bisi, *Appl. Surf. Sci.* **56-58** (1992) 416.
- [41] S. Hüfner, *Photoelectron Spectroscopy* (Springer, Berlin, 1995).
- [42] B.D. Wissman, D.W. Gidley and W.E. Frieze, *Phys. Rev.* **B 46** (1992) 16058.